

Title	Characteristics of Brittle Fracture Under Bi-axial Tensile Load (2nd Report)(Welding Mechanics, Strength & Design)
Author(s)	Ueda, Yukio; Ikeda, Kazuo; Yao, Tetsuya; Aoki, Mitsuru; Shibasaki, Shunichi; Shirakura, Takao
Citation	Transactions of JWRI. 8(1) P.121-P.130
Issue Date	1979-06
Text Version	publisher
URL	<a href="http://hdl.handle.net/11094/8139">http://hdl.handle.net/11094/8139</a>
DOI	
rights	本文データはCiNiiから複製したものである
Note	

*Osaka University Knowledge Archive : OUKA*

<https://ir.library.osaka-u.ac.jp/>

Osaka University

# Characteristics of Brittle Fracture Under Bi-axial Tensile Load (2nd Report)<sup>†</sup>

Yukio UEDA\*, Kazuo IKEDA\*\*, Tetsuya YAO\*\*\*, Mitsuru AOKI\*\*,  
Shunichi SHIBASAKI\*\*\*\* and Takao SHIRAKURA\*\*

## Abstract

In the previous report the brittle fracture initiation characteristics of plate subjected to bi-axial tensile load was investigated on the cruciform specimen of PMMA (polymethylmethacrylate) and SM41 (mild steel), each of which contains an inclined notch. The former specimens fractured in a perfectly brittle manner at room temperature. For the latter specimens, the test temperature was so selected that the fracture occurs in a brittle manner with small scale yielding. In both cases, the fracture stress and the direction of initial crack propagation were well predicted by the criteria based on either maximum tangential stress,  $\sigma_{\theta, \max}$ , or maximum energy release rate  $G_{\theta, \max}$ .

In this report the brittle fracture initiation characteristics with large scale yielding is investigated. A series of fracture tests is conducted on the cruciform specimens of SM41 under bi-axial tensile load, of which load ratios are 0/1, 1/2 and 1/1. Elastic-plastic stress analysis is also carried out using the finite element method. The results obtained by the experiments and the finite element analysis lead to the following conclusions.

- (1) The direction of fracture initiation is nearly normal to the vector of crack opening displacement (COD) near the tip of notch obtained by the finite element analysis.
- (2) Brittle fracture stress under mixed mode conditions may be conservatively predicted by the critical COD for the opening mode fracture as the application of COD-concept.

KEY WORDS: (Brittle Fracture) (Mild Steel) (Unfired Pressure Vessels) (Toughness) (Propagation of cracks)

## 1. Introduction

In general, structures are subjected to external forces in complex manner, and consequently, cracks in structures initiate and propagate in combined modes. In the preceding papers<sup>1) 2)</sup>, the initiation characteristics of brittle fracture from a crack under a complex stress state were investigated. In the previous study, two series of fracture tests were carried out, using the PMMA (Polymethyl-methacrylate) for one series and SM41 (Mild steel) for the other, respectively. The test specimens used were the cruciform type and the rectangular type, each containing an inclined notch, and the bi-axial tensile loads were applied to the former specimens. Then, validity of the several existing fracture criteria were examined based on the test results. The following conclusions were obtained

- (1) In case of perfectly brittle fracture, the fracture stress and the direction of fracture initiation are well predicted by the criteria based on the maximum tangential stress ( $\sigma_{\theta, \max}$ )<sup>3)</sup> and the maximum

decreasing rate of the total potential energy ( $G_{\theta, \max}$ )<sup>4)</sup>.

- (2) In case of brittle fracture with small scale yielding, the direction of fracture initiation is well predicted by the criterion of  $G_{\theta, \max}$ , but the predicted fracture stresses are somewhat lower than the test results.

In this report, brittle fracture under combined modes of Mode I (opening) and Mode II (sliding) is investigated accompanying large scale yielding and also at the general yielding state. First, a series of fracture test under bi-axial tensile loads is carried out using the cruciform type specimens of SM41 with an inclined notch. Elastic-plastic stress distributions in the vicinity of the notch are obtained by means of the finite element method. Then, the COD concept newly extended to the case of a crack under mixed mode condition is examined, based on the results obtained by the fracture test and stress analysis.

<sup>†</sup> Received on March 31, 1979

\* Professor

\*\* Structural Engineering Laboratory, Kobe Steel, Ltd.

\*\*\* Instructor

\*\*\*\* Graduate Student

2. Experiment

2.1 Material and test specimens

The mechanical properties and the chemical composition of mild steel, SM41, supplied are represented in Table 1. The specimen is of a cruciform type, containing a center notch which is inclined at an angle,  $\beta$ , to the vertical direction, and is machined through the thickness of the plate. The details of the test specimen are shown in Fig. 1.

Table 1 Mechanical properties and chemical composition

Material	Mechanical properties			Chemical composition (%)				
	$\sigma_s$ (kg/mm <sup>2</sup> )	$\sigma_B$ (kg/mm <sup>2</sup> )	EL.	SiC	Si	Mn	P	S
SM41	41	50	26	0.14	0.25	0.86	0.028	0.014

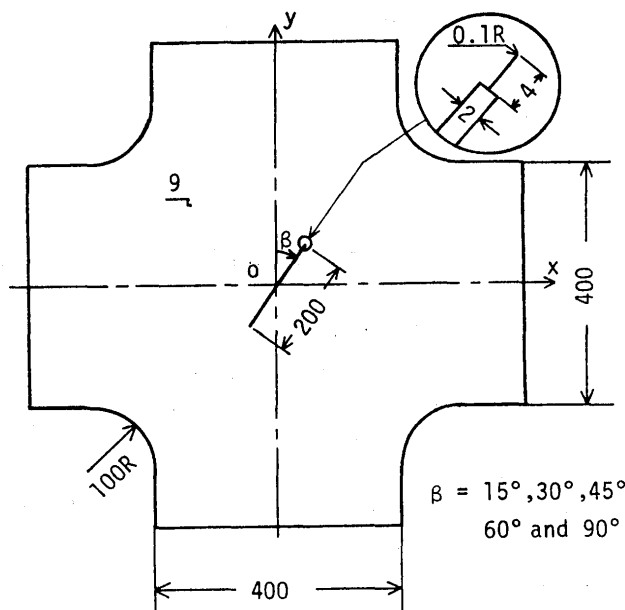


Fig. 1 Test specimen

2.2 Test procedure

A series of the fracture test is conducted at the temperature range between  $-60^\circ\text{C}$  and  $-90^\circ\text{C}$ . The specimens are fractured in brittle manner, being subjected to large scale yielding or general yielding. A vertical testing machine of 300 tons is used, with a combination of a specially designed horizontal testing machine of 150 tons which can move in accordance with the vertical displacement of the specimen<sup>1)</sup>.

In the test, the direction of propagation of the initial crack and the fracture load are measured. The crack

opening displacement, COD, is also measured during loading by clip-gages. Two clip-gages are attached to the specimen between A, B and A, C in Fig. 2. Small circular holes are machined at points A, B and C, where the clip-gages are attached. Point A is 30 mm apart from the tip of notch. COD under a mixed mode condition can be separated into two components,  $V_I$  and  $V_{II}$ , which correspond to those for mode I and mode II, respectively. Assuming that the distance between B and C does not change, each COD is graphically obtained by measuring the distances  $\overline{BA'}$  and  $\overline{CA'}$  in Fig. 2.

Deep notch tests are also carried out at the temperature range between  $-60^\circ\text{C}$  and  $-90^\circ\text{C}$ , and the fracture toughness (critical crack opening displacement,  $\Phi_c$ ) is evaluated from the test results in addition to the previous ones<sup>1)</sup>.

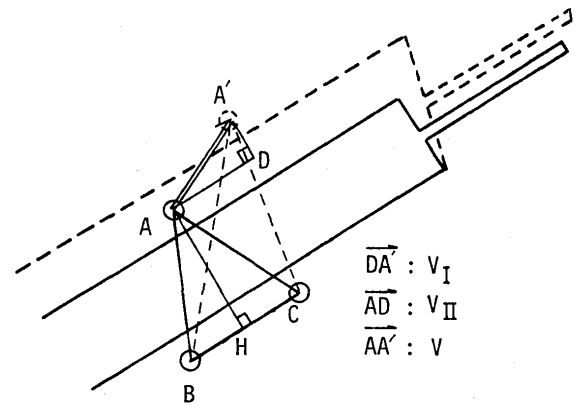


Fig. 2 Measurement of COD under mixed mode

3. Elastic-plastic stress analysis

3.1 Finite element analysis

A series of elastic-plastic stress analysis is carried out to obtain the crack opening displacement by the finite element method employing the constant strain element. Different finite element meshes are employed according to the notch inclination angle,  $\beta$ . However, mesh size near the tip of notch is kept the same regardless to  $\beta$  and bi-axial load ratio,  $P_x/P_y$ , and the meshes for analysis is shown in Fig. 3. In the analysis, substructure method is employed to save computer time and labor for generation of the input data. The analysis is performed on the test specimens for all possible combinations of the notch inclination angle ( $\beta = 15^\circ, 30^\circ, 45^\circ, 60^\circ$  and  $90^\circ$ ) and the bi-axial load ratio ( $P_x/P_y = 0/1, 1/2$  and  $1/1$ ). Young's modulus,  $E$ , strain hardening rate,  $H'$ , and yield stress,  $\sigma_s$ , are assumed to be 21,000 kg/mm<sup>2</sup>, 210 kg/mm<sup>2</sup> and 30 kg/mm<sup>2</sup>, respectively, and von Mises's yield condition is employed.

3.2 Elastic-plastic behavior of the specimen

The calculated mean stress-COD curves and the plastic zone sizes for all cases are represented in Fig. 3. The mean stress,  $\sigma_y$  is nondimensionalized by the yield stress  $\sigma_s$ , and COD,  $\Phi$ , by  $\sigma_s, E$ , and a half length of the notch,  $c$ . Crack opening displacement,  $\Phi$ , under mixed mode condition is defined as the vector which is composed of the displacement in mode I,  $\Phi_{I,0.5}$ , and that in mode II,  $\Phi_{II,0.5}$ , at a distance of 0.5 mm apart from the tip of notch. This compound COD vector inclines to the notch

line by an angle of  $\tan^{-1} (\Phi_{I,0.5}/\Phi_{II,0.5})$  and its magnitude is equal to  $\sqrt{\Phi_{I,0.5}^2 + \Phi_{II,0.5}^2}$ . For all notch angles, spreads of plastic zone and  $\Phi E/\sigma_s c \sim \sigma/\sigma_s$  curves are almost the same when  $P_x/P_y = 0/1$ . However, the development of the plastic zone from the tip of the notch under a mixed stress mode is very complex. The shape or spread of calculated plastic zone is influenced by the notch angle,  $\beta$ , and the bi-axial load ratio,  $P_x/P_y$ , and consequently, the crack opening behavior is very complex, when  $P_x/P_y$  is not equal to 1.

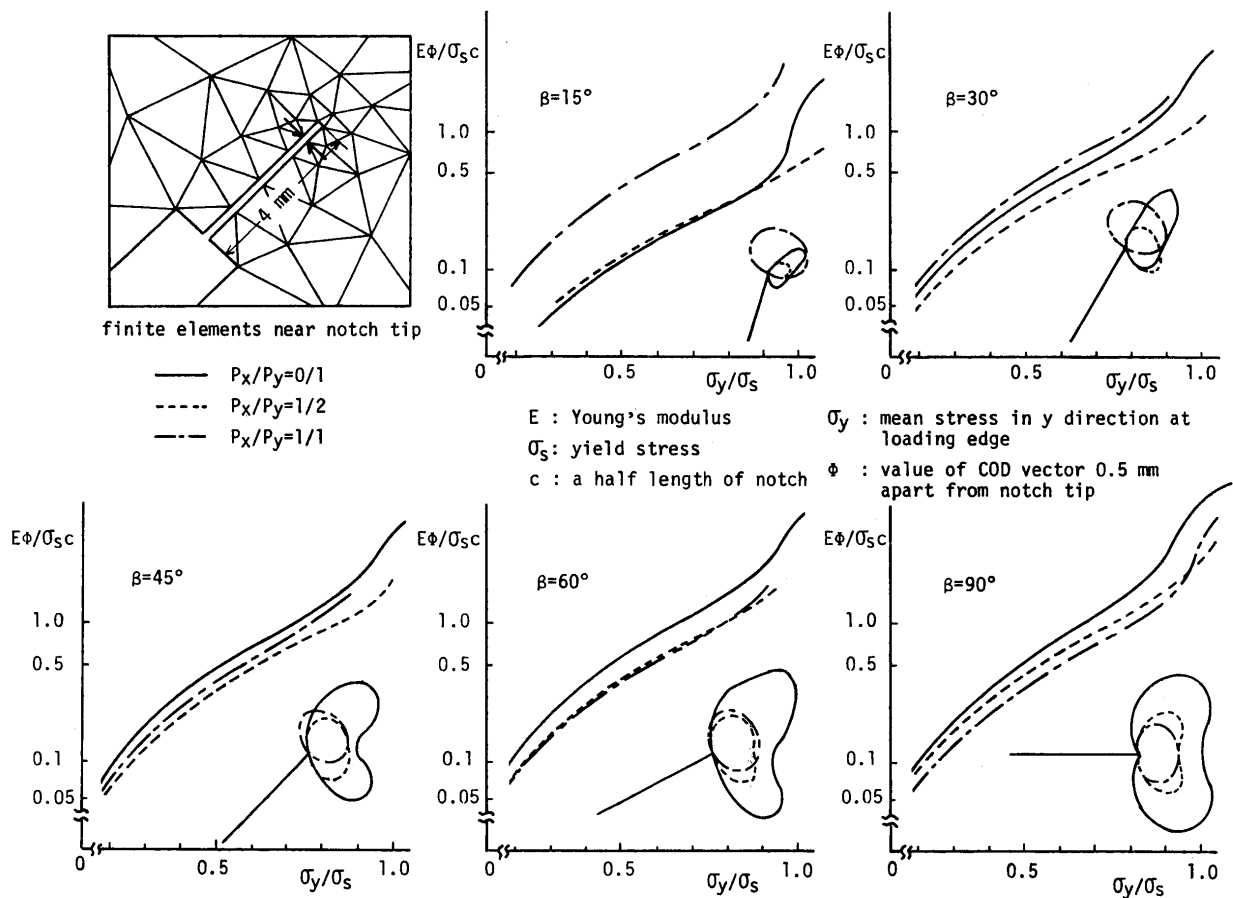


Fig. 3 Mean stress - COD curves and spread of plastic zone ( $\sigma_y/\sigma_s = 0.75$ )

3.3 Mean stresses around a notch

The mean stresses  $\sigma_{xe}$  and  $\sigma_{ye}$  around the notch are in general different from  $\sigma_x$  and  $\sigma_y$  along the loading edges in the case of the cruciform specimen as shown in Fig. 4. In the case of a notch being 160 mm long, reported in the previous paper, the stress ratios,  $\sigma_{xe}/\sigma_x$  and  $\sigma_{ye}/\sigma_y$  were the same regardless to the notch angle,  $\beta$ , when the specimen is in the elastic state. However, in the case of a notch being 200 mm long in this study, these stress ratios vary somewhat according to the notch angle,  $\beta$ , and the

bi-axial load ratio,  $P_x/P_y$ . Figure 5 shows such variation, and it is observed that the stress ratios increases slightly with  $\sigma_y$  when  $\sigma_y/\sigma_s > 0.5$ . The stress ratio,  $\sigma_{xe}/\sigma_x$ , has the same tendency with  $\sigma_x$ , but it is confirmed that the stress ratio,  $\sigma_{xe}/\sigma_{ye}$  does not change even when  $\sigma_x/\sigma_s$  or  $\sigma_y/\sigma_s$  is greater than 0.5. Consequently, it may be said that  $\sigma_{xe}/\sigma_{ye}$  is -0.09, 0.41 and 1.0 when  $P_x/P_y$  is 0/1, 1/2 and 1/1, respectively, which are the same values to those in the previous report<sup>1)</sup>.

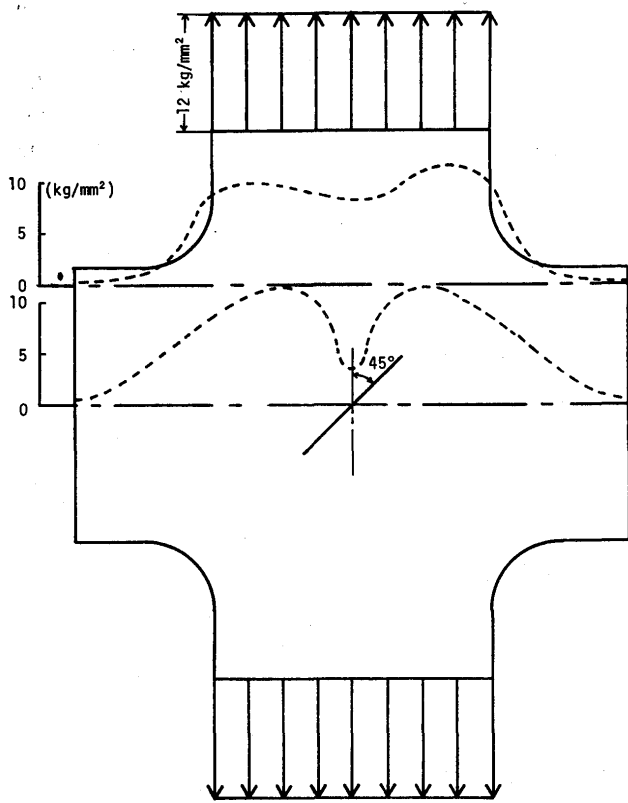


Fig. 4 Stress distribution in cruciform specimen

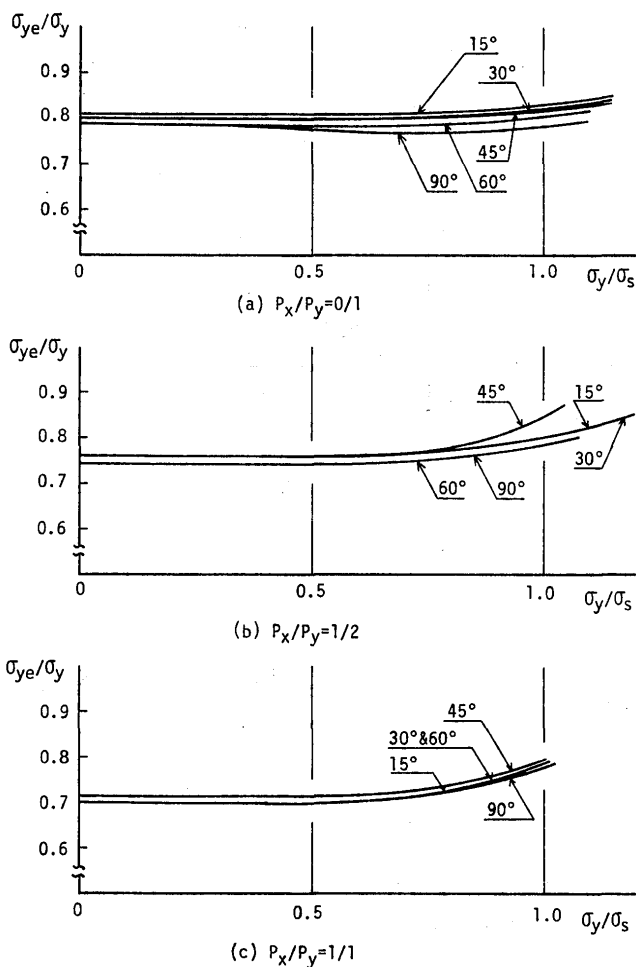


Fig. 5 Field stress versus applied stress (y direction)

#### 4. Test results and discussion

##### 4.1 Non-dimensionalization of the calculated results

Fracture tests are carried out at various temperatures. The test temperature influences the yield stresses of the material. Therefore, stress analysis of each specimen under loading should be performed with the corresponding value of the yield stress to the test temperature. This requires a plenty of computation time. Here, a new procedure of the analysis is proposed based on the following theory, which reduces the repetition of the similar analysis for different materials.

First, the following assumption is made that Young's modulus,  $E$ , Poisson's ratio,  $\nu$ , and the strain hardening ratio,  $H'$ , are not dependent on temperature. Now, consider two same specimens in shape but they are made of two different kinds of steel, steel (A), and steel (B), of which yield stresses,  $\sigma_{s1}$  and  $\sigma_{s2}$ , are different in magnitude. With the above mentioned assumptions, the stress-strain curves for these two materials are drawn in Fig. 6(a). For Fig. 6(a), the bi-linear relation is employed for simplicity. However, any other type may be used if  $H'/E$  and  $\bar{\epsilon}/\epsilon_s$  relations are same for both steels (note:  $\bar{\epsilon}$  and  $\epsilon_s$  are the equivalent strain and yield strain).

For elastic-plastic analysis, the incremental method is employed. Each load increment is so chosen that one element yields at each step. For the first load increment all elements are elastic, and their stiffness matrices for both specimens are same. After the first load increment is applied, one element is yielded, and the equivalent stresses and strains in both specimens are represented by  $\bar{\sigma}_{1,1}$ ,  $\bar{\sigma}_{2,1}$  and  $\bar{\epsilon}_{1,1}$ ,  $\bar{\epsilon}_{2,1}$ , which correspond to points  $a_1$  ( $\bar{\epsilon}_{1,1}$ ,  $\bar{\sigma}_{1,1}$ ) and  $b_1$  ( $\bar{\epsilon}_{2,1}$ ,  $\bar{\sigma}_{2,1}$ ) in Fig. 6(a), respectively. Equivalent stress,  $\bar{\sigma}_{1,1}$  or  $\bar{\sigma}_{2,1}$  is obviously equal to the yield stress,  $\sigma_{s1}$  or  $\sigma_{s2}$ . Then, the magnitude of stress components  $\sigma_x$ ,  $\sigma_y$  and  $\tau_{xy}$ , in one specimen is proportional to that in the other one by the ratio of the yield stresses. Therefore, the ratio of  $\sigma_x/\sigma_y$ ,  $\sigma_y/\tau_{xy}$ , in one specimen is the same as in the other one. The load-displacement curves for both specimens are shown in Fig. 6(b), where points  $A_1$  ( $u_{1,1}$ ,  $P_{1,1}$ ) and  $B_1$  ( $u_{2,1}$ ,  $P_{2,1}$ ) correspond to points  $a_2$  and  $b_2$  on the  $\bar{\sigma}$ - $\bar{\epsilon}$  curves, respectively, It is found that

$$P_{1,1}/P_{2,1} = u_{1,1}/u_{2,1} = \sigma_{s1}/\sigma_{s2} \quad (1)$$

For the second load increment, one element in each specimen is plastic, for which the plastic stiffness matrix should be used. In the plastic range, the stress-strain relation at plane stress state is expressed in the following incremental form<sup>5)</sup>,

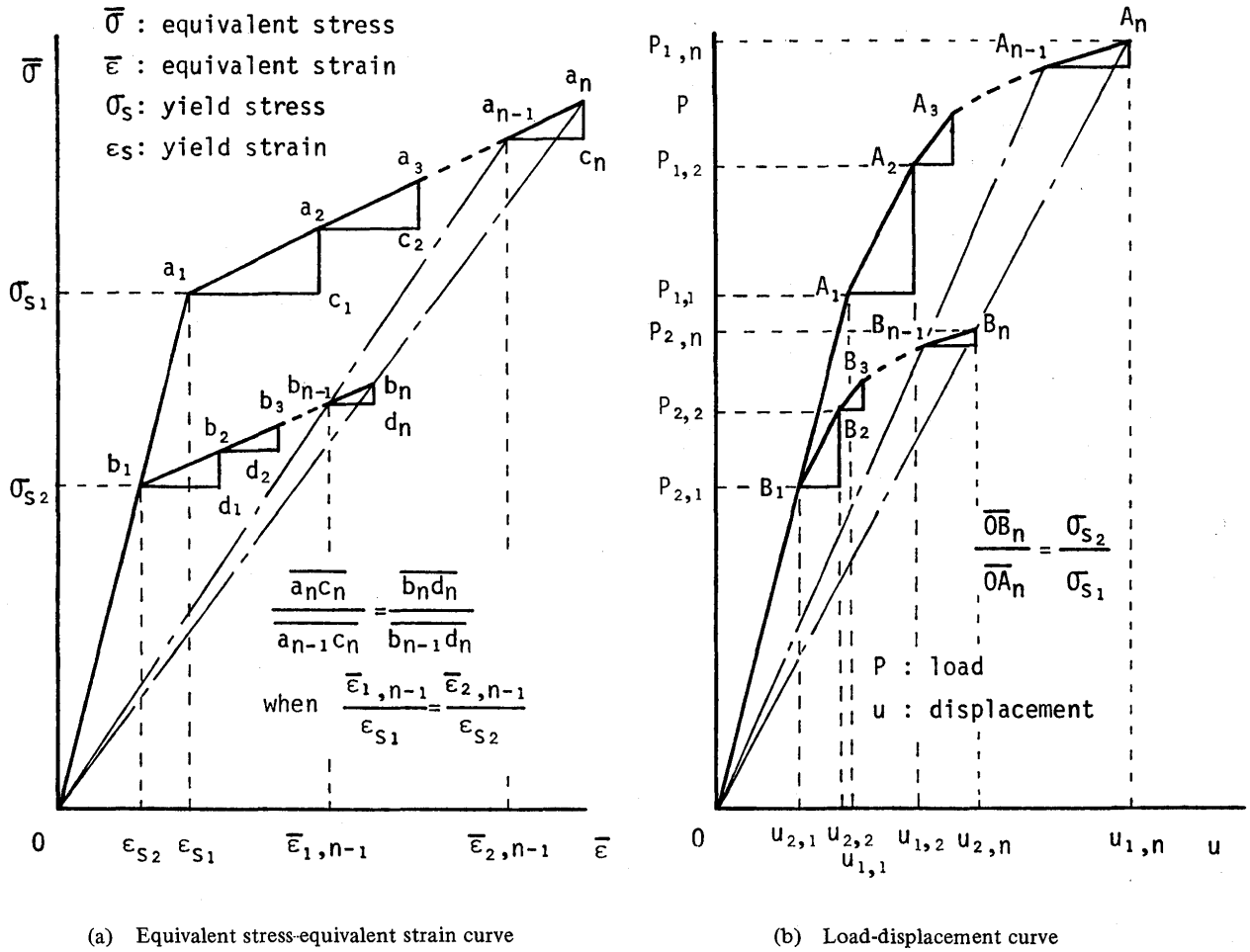


Fig. 6 Assumed stress-strain relation and resulting load-displacement relation

$$\begin{Bmatrix} d\sigma_x \\ d\sigma_y \\ d\tau_{xy} \end{Bmatrix} = [D^P] \begin{Bmatrix} d\epsilon_x \\ d\epsilon_y \\ d\gamma_{xy} \end{Bmatrix} \quad (2)$$

where

$$[D^P] = \begin{bmatrix} \frac{E}{1-\nu^2} - \frac{S_1^2}{S} & & \\ & \text{SYM.} & \\ \frac{\nu E}{1-\nu^2} - \frac{S_1 S_2}{S} & \frac{E}{1-\nu^2} - \frac{S_2^2}{S} & \\ & & \frac{E}{2(1+\nu)} - \frac{S_3^2}{S} \end{bmatrix}$$

$$S_1 = \frac{E}{1-\nu^2} (\sigma'_x + \nu \sigma'_y), \quad S_2 = \frac{E}{1-\nu^2} (\sigma'_y + \nu \sigma'_x),$$

$$S_3 = \frac{E}{1-\nu^2} \tau_{xy}, \quad S = \frac{2}{3} E \sigma^2 \left\{ 1 + \frac{2(1+\nu)H'}{3E} \right\},$$

$$\sigma^2 = \sigma_x^2 - \sigma_x \sigma_y + \sigma_y^2 + 3\tau_{xy}^2,$$

$$\sigma'_x = \frac{1}{3} (2\sigma_x - \sigma_y), \quad \sigma'_y = \frac{1}{3} (2\sigma_y - \sigma_x)$$

It is observed that the plasticity matrix is dependent upon the ratios of the stress components, such as  $\sigma_x/\sigma_y$  and  $\sigma_y/\tau_{xy}$ , and  $H'/E$ , but the yield stress. In both specimens,  $H'/E$  and the ratio of stress components in the corresponding elements are same. If these conditions are introduced in Eq. (2), it is found that the plasticity matrix is completely same for both specimens. Consequently, the corresponding stiffness matrices of the plastic elements are same. For the analysis to the second load increment, the stiffness matrices of all elements for the specimen are superposed. These resulting whole stiffness matrices for both specimens are same, since all

corresponding element stiffness matrices are same for both specimens.

After the second load increment is applied the loads and displacements of both specimens are  $P_{1,2}$ ,  $P_{2,2}$  and  $u_{1,2}$ ,  $u_{2,2}$ , which correspond to points  $A_2$  ( $u_{1,2}$ ,  $P_{1,2}$ ) and  $B_2$  ( $u_{2,2}$ ,  $P_{2,2}$ ) in Fig. 6(b). The relation between load and displacement increments of both specimens is same, because their stiffness matrices are same, and

$$dP_{1,2}/du_{1,2} = dP_{2,2}/du_{2,2} \quad (3)$$

The magnitude of these increments are determined by the condition of yielding of a element (or elements) depending on the yield stresses, and

$$dP_{1,2}/dP_{2,2} = du_{1,2}/du_{2,2} = \sigma_{s1}/\sigma_{s2} = a \quad (4)$$

Therefore, the magnitude of the total load and displacement at point  $A_2$  ( $u_{1,2}$ ,  $P_{1,2}$ ) are greater than that at point  $B_2$  ( $u_{2,2}$ ,  $P_{2,2}$ ), by the ratio of  $\sigma_{s1}/\sigma_{s2}$  since

$$P_{2,2} = P_{2,1} + dP_{2,2} = a (P_{1,1} + dP_{1,2}) = aP_{1,2} \quad (5)$$

$$u_{2,2} = u_{2,1} + du_{2,2} = a (u_{1,1} + du_{1,2}) = au_{1,2}$$

The equivalent stress and strain increments of the firstly yielded element in both specimens are  $d\bar{\sigma}_{1,2}$ ,  $d\bar{\sigma}_{2,2}$  and  $d\bar{\epsilon}_{1,2}$ ,  $d\bar{\epsilon}_{2,2}$ , and

$$d\bar{\sigma}_{1,2}/d\bar{\sigma}_{2,2} = d\bar{\epsilon}_{1,2}/d\bar{\epsilon}_{2,2} = \sigma_{s1}/\sigma_{s2} \quad (6)$$

Consequently,

$$\bar{\sigma}_{2,2} = \bar{\sigma}_{2,1} + d\bar{\sigma}_{2,2} = a (\bar{\sigma}_{1,1} + d\bar{\sigma}_{1,2}) = a\bar{\sigma}_{1,2} \quad (7)$$

$$\bar{\epsilon}_{2,2} = \bar{\epsilon}_{2,1} + d\bar{\epsilon}_{2,2} = a (\bar{\epsilon}_{1,1} + d\bar{\epsilon}_{1,2}) = a\bar{\epsilon}_{1,2}$$

and the ratio of stress components,  $\sigma_x/\sigma_y$  and  $\sigma_y/\tau_{xy}$ , in the corresponding elements are same. Therefore, the plastic stiffness matrices of the corresponding elements in both specimens are completely same.

The same relation exists for the subsequent load increments, and the following relation is obtained between load increments,  $dP_{1,n}$  and  $dP_{2,n}$ , and displacement increments,  $du_{1,n}$  and  $du_{2,n}$ , at the  $n$ -th step,

$$dP_{1,n}/dP_{2,n} = du_{1,n}/du_{2,n} = \sigma_{s1}/\sigma_{s2} \quad (8)$$

and, consequently,

$$P_{1,n}/P_{2,n} = u_{1,n}/u_{2,n} = \sigma_{s1}/\sigma_{s2} \quad (9)$$

where

$$P_{1,n} = \sum_{i=1}^n dP_{1,i}, \quad P_{2,n} = \sum_{i=1}^n dP_{2,i} \quad (10)$$

$$u_{1,n} = \sum_{i=1}^n u_{1,i}, \quad u_{2,n} = \sum_{i=1}^n u_{2,i}$$

Furthermore, the plastic stiffness matrix is proportional to Young's modulus,  $E$ , as is known from Eq. (2). Therefore, the whole stiffness matrix of the specimen is proportional to  $E$ , and

$$\{P\} = E [K'] \{u\} \quad (11)$$

where,  $E [K']$  is the whole stiffness matrix. Deviding the both terms of Eq. (11) by  $c \cdot A \cdot \sigma_s$ , the following equation is obtained

$$\left\{ \frac{P}{A\sigma_s} \right\} = \frac{c}{A} [K'] \left\{ \frac{Eu}{\sigma_s c} \right\} \quad (12)$$

where  $c$  and  $A$  are a half length of notch and the cross sectional area of the specimen, respectively.  $P/A\sigma_s = \sigma_y/\sigma_s$  and  $Eu/\sigma_s c$  in Eq. (12) are the non-dimensionalized mean stress and displacement. Here, replacing  $u$  by the crack opening displacement,  $\Phi$ , Eq. (12) becomes

$$\left\{ \sigma_y/\sigma_s \right\} = [K''] \left\{ E\Phi/\sigma_s c \right\} \quad (13)$$

where  $[K''] = c/A \cdot [K']$ . It is found that the relation between  $\sigma_y/\sigma_s$  and  $E\Phi/\sigma_s c$  is completely same for any specimen being same in shape and notch length but young's modulus and yield stress, provided that  $H'/E$  and  $\bar{\epsilon}/\epsilon_s$  relation is same.

#### 4.2 Comparison between observed and theoretically calculated CODs

COD was measured at a position 30 mm apart from the tip of notch for several cases where the load ratio,  $P_x/P_y$ , and the notch angle,  $\beta$ , are changed. For the case of  $\beta = 30^\circ$  at  $P_x/P_y = 0.1$ , the observed and calculated CODs are shown against the applied load in Fig. 7. In the analysis, the variation of the yield stress,  $\sigma_s$ , according to the testing temperature is taken into consideration by the procedure described in section 4.1. As the load exceeds about 100 ton, the experimental COD becomes greater than the calculated one. If there exists short slow crack growth at the actual notch, this might increase the value of COD. Taking this into account, the measured COD is considered to agree well with the analyzed one.

Anyhow, it is difficult to measure COD under mixed mode loading at the test and it is complicated to convert the measured COD to that at the notch tip. In the

following discussion, the calculated COD vector at the position 0.5 mm apart from the tip of notch is regarded as that at the tip of notch as shown in Fig. 3.

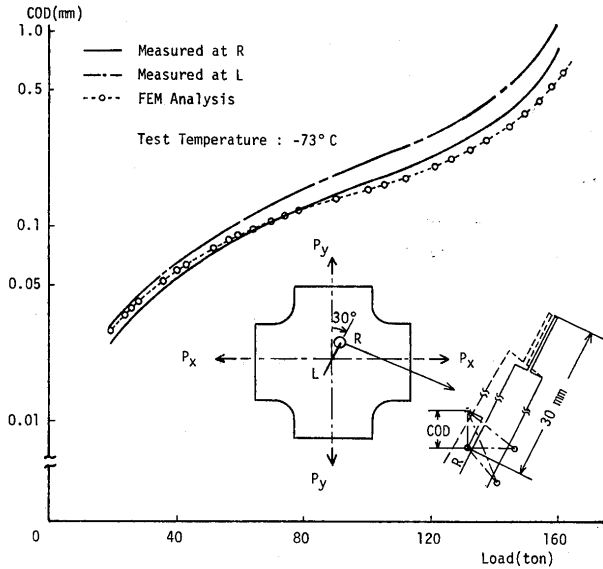


Fig. 7 Comparison of measured COD with calculated one

4.3 Direction of crack initiation

The relationship between the notch angle,  $\beta$ , and direction of propagation of the crack with respect to the initial notch angle,  $-\theta$ , is shown in Figs. 8(a), (b) and (c) for load ratios,  $P_x/P_y = 0/1, 1/2$  and  $1/1$ , respectively. In the case of  $\beta = 15^\circ, 30^\circ$  and  $45^\circ$  at  $P_x/P_y = 0/1$ , the fracture initiates in a direction of  $\beta + (-\theta) = 45^\circ$ , that is, the direction of the maximum shear stress in the plate without a notch. The fracture surface is normal to the plate surface and shows shear appearance. Hereafter, this type of fracture is referred to as shear fracture. Microscopic observation of the shear appearance is discussed in the subsequent section, 4.6. The solid lines in Fig. 8 show the direction of propagation of the crack estimated from the assumption that the fracture initiates in the direction perpendicular to the COD vector obtained by the elasto-plastic analysis of FEM. The estimated line for  $P_x/P_y = 1/1$  coincides with the horizontal axis in Fig. 8.

The estimated directions show good agreement with the observed ones except in the case of the shear fracture. This agreement will be attributed to the fact that the COD vector at the tip of notch is closely related to the vector of the stretched zone depth formed prior to the fracture, and that the fracture initiates in the direction perpendicular to the stretched zone<sup>6)</sup>.

In contrast with this, the maximum energy release rate

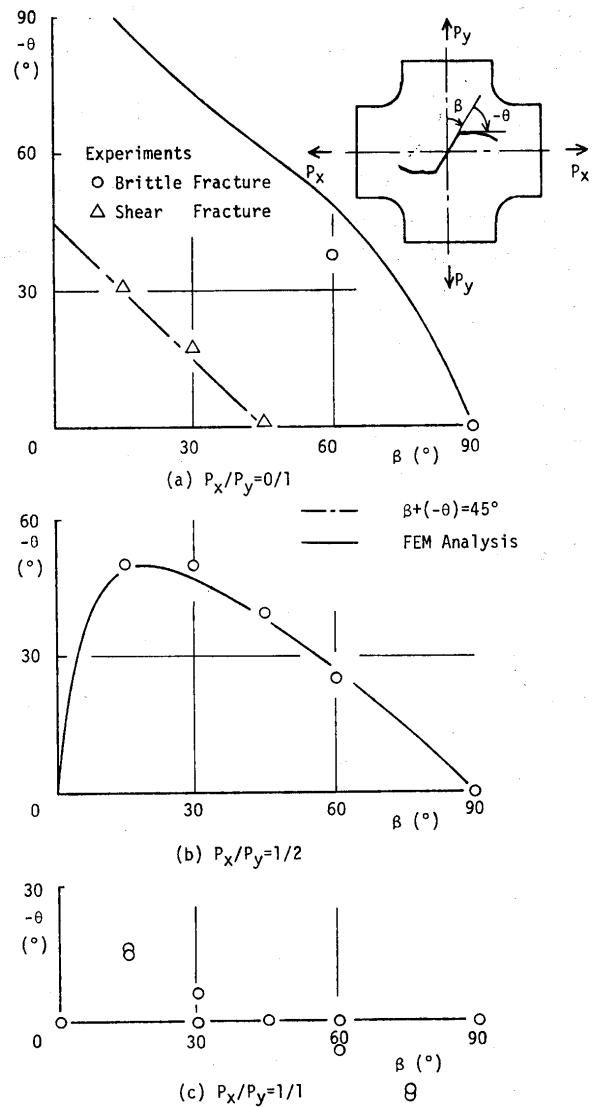


Fig. 8 Direction of crack propagation (large scale yielding)

criterion,  $G_{\theta, \max}$ , and the COD vector criterion can be applied for prediction of the direction of the fracture initiation from a notch with small scale yielding under mixed mode loading. The direction which is predicted by the former criterion, that is,  $G_{\theta, \max}$  shows better agreement with the observed direction than that by the latter COD criterion.

In the above two cases, the extent and size of the yielded zone at the tip of notch under mixed mode loading are different. Judging from the result of comparison, it is recognized that each criteria should be applied to an appropriate case. From this conclusion, the direction of the fracture initiation from the notch with small scale yielding should be predicted by the  $G_{\theta, \max}$  criterion, based on energy balance. On the other hand, in the case of being accompanied by large scale yielding or general yielding, the direction can be predicted by the



COD criterion, based on deformation at the tip of notch.

Moreover, when the specimen is subjected to pure Mode II at such temperature range as brittle fracture of pure Mode I with large scale yielding or general yielding occurs, the COD vector becomes parallel to the notch. Therefore, the direction of fracture initiation will be estimated to be perpendicular to the notch. However, in fact, the shear crack from the tip of notch precedes prior to complete fracture. Therefore, the behavior to fracture is anticipated to be more complicated.

4.4 Fracture stress

Variation of the fracture stress for different notch angle is represented in Fig. 9. The vertical coordinate is

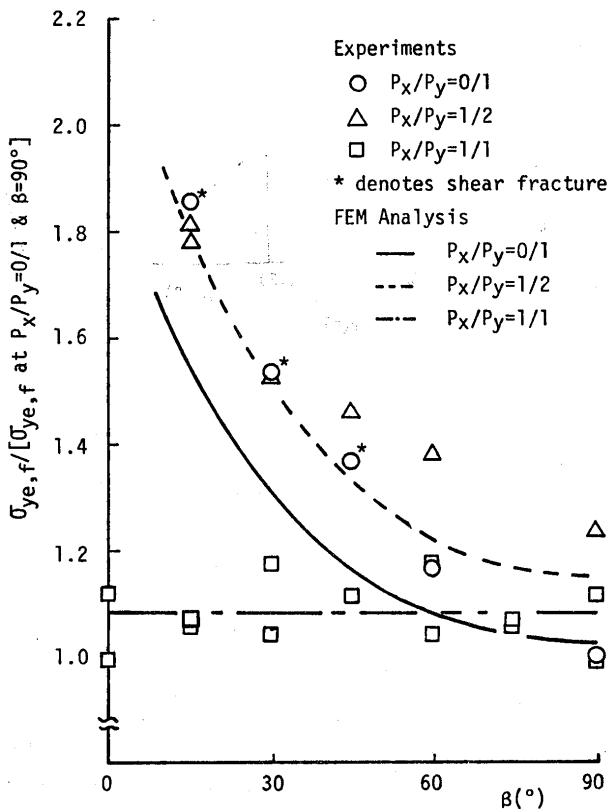


Fig. 9 Variation of fracture stress with notch angle

the ratio of the effective fracture stress in the y-direction at the central part of the specimen,  $\sigma_{ye,f}$ , to that for  $\beta = 90^\circ$  and  $P_x/P_y = 0/1$ . As explained above, the fracture for  $\beta = 15^\circ, 30^\circ$  and  $45^\circ$  under  $P_x/P_y = 0/1$  was the shear type, and the maximum stress is indicated, which does not correspond to the fracture load. (The test specimen did not fracture completely.) While the fracture stress for  $P_x/P_y = 0/1$  and  $1/2$  increases with a decrease of  $\beta$ , that for  $P_x/P_y = 1/1$  is kept nearly constant irrespective of  $\beta$ . The lines in Fig. 9 denote the estimated fracture stresses based on the COD criterion which will be discussed in the

following section. The experimental fracture stresses under pure Mode I, that is, for  $P_x/P_y = 1/1$  or  $\beta = 90^\circ$ , are plotted in the neighborhood of the estimated line. On the other hand, those under various mixed mode conditions, which are, for  $\beta \neq 90^\circ$ , and  $P_x/P_y = 0/1$  or  $1/2$ , scatter a little above the estimated lines.

4.5 Application of COD criterion to mixed mode conditions

The COD concept has been proposed as a fracture criterion especially in the field of the fracture with large scale yielding or general yielding under pure Mode I and pure Mode III conditions, and the applicability of that concept has been verified. In parallel with this, the strip yield model has been proposed as an elasto-plastic crack model for calculation of COD by Dugdale<sup>7)</sup> and Bilby *et al*<sup>8)</sup>. Moreover, even the strip yield model under mixed mode loading is proposed by Sakai and Sakano<sup>9)</sup>. In these strip yield models, COD can be determined from the condition that the stress singularity vanishes at the tip of the plastic region on the prolonged line of the notch. Therefore, since stress singularity does not occur under uniform tension applied parallel to the notch, such as  $\sigma_x$  in the case of being  $\beta = 90^\circ$ , the size of the plastic region is not dependent upon  $\sigma_x$ . However, as shown in Fig. 3,

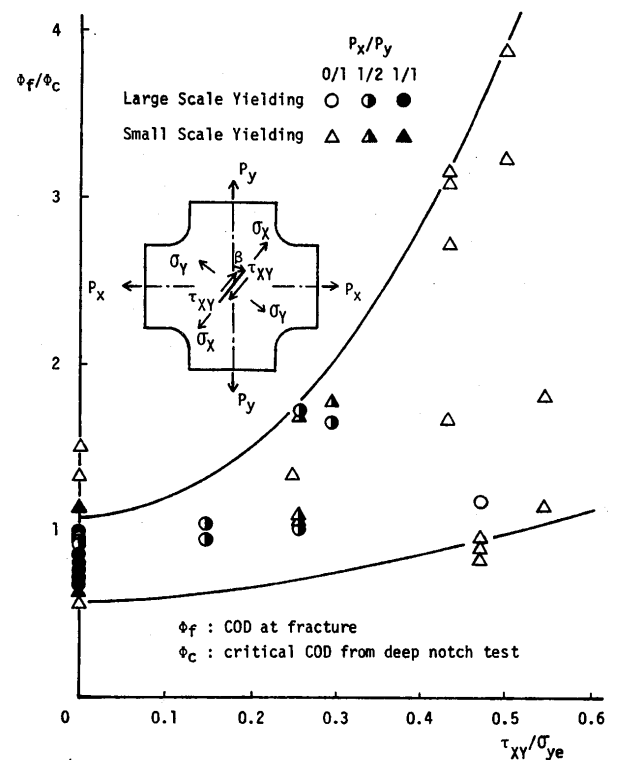


Fig. 10 Variation of COD at fracture with shear stress parallel to notch

Fig. 10 Variation of COD at fracture with shear stress parallel to notch

the actual size of the plastic zone is significantly influenced by the magnitude of  $\sigma_x$ , and so is COD. Thus, the size of the plastic zone in the strip yield model is not actual but conceptual, and this indicates a reasonable value only for the limiting case of being  $\beta = 90^\circ$  at  $P_x/P_y = 0/1$ . Essentially, the size and extending direction of the plastic zone should be related closely to COD. However, it is very difficult to take into account of the respective component of stress in the dynamical model of COD proposed so far. To this point, COD under mixed mode conditions was analyzed by FEM, and the applicability of COD concept was investigated.

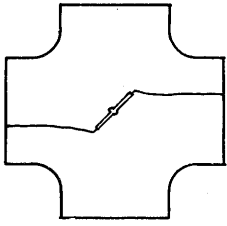
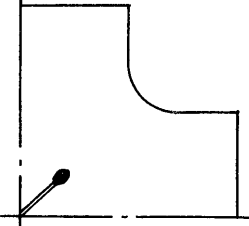
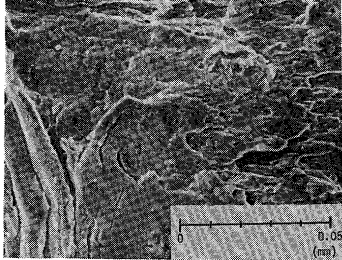
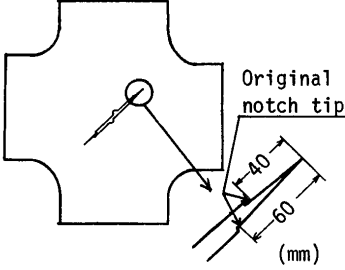
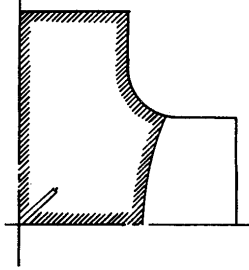
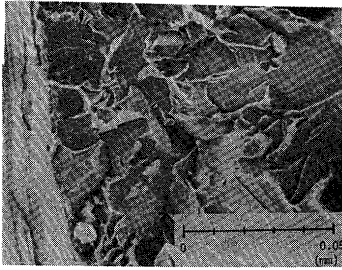
As reported previously<sup>1)</sup>, the test results of the brittle fracture with small scale yielding under the mixed mode conditions revealed that the critical fracture parameter,  $G_{cr}$ , tends to increase with an increase of  $K_{II}$ , which is the stress intensity factor corresponding to Mode II. From the results of experiment and analysis by FEM, the ratio of CODs,  $\Phi_f/\Phi_c$ , is plotted against the non-dimensionalized shear stress,  $\tau_{xy}/\sigma_{ye}$ , in Fig. 10. Here,  $\Phi_f$  denotes the COD at fracture, which is determined from the relation

shown in Fig. 3, with introducing the fracture stress, and  $\Phi_c$  denotes the critical COD at the corresponding test temperature from the deep notch test. In this figure, the result of fracture with small scale yielding by the previous test is also shown. This figure indicates that  $\Phi_f$  increases with an increase of the shear stress in the same manner as  $G_{cr}$ . Therefore, as shown in Fig. 9, the actual fracture stresses under the mixed mode loading are higher than the estimated ones which are calculated based on the COD criterion. That is, the component of COD corresponding to Mode II is not so influential to brittle fracture of elastic-plastic material as the corresponding component to Mode I. This problem should be studied also from microscopic aspect in the future. However, as the estimated fracture strength under mixed mode loading is conservative, such estimation by the COD concept is practically effective.

4.6 Shear fracture

As stated in the section 4.3, the shear fracture initiated from the tip of notch in the cases of being  $\beta = 15^\circ, 30^\circ$  or

Table 2 Comparison of shear fracture with brittle fracture

Type of Fracture	Crack Propagation Pattern	Spread of Plastic Zone at Fracture	Fractograph
Brittle Fracture $\beta=45^\circ$ $P_x/P_y=0/1$ Test Temp.: $-140^\circ\text{C}$			
Shear Fracture $\beta=45^\circ$ $P_x/P_y=0/1$ Test Temp.: $-75^\circ\text{C}$			

$45^\circ$  and  $P_x/P_y = 0/1$ . In this section, the shear fracture is characterized by comparing it with the brittle one. As an example, the case of  $\beta = 45^\circ$  and  $P_x/P_y = 0/1$ , a comparison between the brittle fracture at  $-140^\circ\text{C}$  and the shear one at  $-75^\circ\text{C}$  is made. Table 2 represents the crack propagation pattern, the plastic zone at fracture and the microphotograph at the tip of notch. In the shear fracture, the plastic zone extends nearly all over the test specimen at fracture, the horizontally sliding displacement between the upper and lower surface of the notch is produced and the crack propagates in the same direction as the maximum shear stress of a specimen without a notch. The average shear stress along the prolonged line of the shear crack is nearly equal to a half of the tensile strength. Moreover while cleavage appearance can be seen at the tip of notch of the specimen fractured in brittle manner, there can be observed the large stretched zone at the tip of notch and the elongated dimple pattern at the propagated part of the crack in the shear manner. Since the equi-axised dimple pattern can be hardly seen in the shear fracture, the component of the shear stress parallel to the shear crack is considered to play the predominant role in such fracture behavior.

## 5. Conclusion

The brittle fracture tests of the cruciform specimen of mild steel with an inclined notch were conducted, being applied bi-axial tension at such temperatures as the double edge notched specimen or the deep notch test specimen fractures with large scale yielding. The results of the fracture with small scale yielding by the previous test as well as those by the present one were compared with the elastic-plastic behaviors of the specimens analysed by FEM.

The following conclusions were drawn:

- (1) The extent of the plastic zone at the tip of notch and the crack opening displacement (COD) under mixed mode loading were obtained by the elastic-plastic stress analysis with the aid of FEM. It was found that when Poisson's ratio, Young's modulus and the strain hardening rate of a material are the same as those of other material, the COD in each case could be normalized by its yield strength.

- (2) The fracture with small scale yielding under mixed mode loading initiates in direction as the energy release rate,  $G_\theta$ , becomes maximum and that with large scale yielding or general yielding initiates perpendicularly to the COD vector analyzed by FEM.
- (3) The COD at the fracture,  $\Phi_f$ , calculated by FEM increases with an increase of the shear stress parallel to the notch in the same manner as  $G_\theta$  at the fracture with small scale yielding,  $G_{cr}$ , apparently increases with an increase of the stress intensity factor corresponding to Mode II,  $K_{II}$ .
- (4) The brittle fracture strength under mixed mode loading can be estimated conservatively on the bases of the COD criterion, in which the COD as a function of the load is analyzed by FEM and the critical COD is obtained from the deep notch test. Therefore, such estimation is considered to be effective from a viewpoint of practical design.

## References

- 1) Y. Ueda, K. Ikeda, T. Yao, M. Aoki, T. Yoshie and T. Shirakura; Brittle Fracture Initiation Characteristics under Bi-axial Loading, J. Soc. Naval Arch. of Japan, Vol. 139 (1976), pp. 240-247., IIW, Doc., X-812-76., Fracture 1977, Vol. 2, ICF4, Waterloo, Canada (1977), pp. 173-181.
- 2) Y. Ueda, K. Ikeda, T. Yao, M. Aoki, T. Yoshie and T. Shirakura; Characteristics of Brittle Fracture under Bi-axial Tensile Load, Trans. JWRI, Vol. 5, No. 2 (1976), pp. 69-77.
- 3) F. Erdogan and G. C. Sih; On the Crack Extension in Plates under Plane Loading and Transverse Shear, Trans., ASME, J. Basic Eng., 85D (1963), pp. 519-527.
- 4) G. P. Anderson, V. L. Ruggles and G. Stibor; Use of Finite Element Computer Programs in Fracture Mechanics Int. J. Fr. Mech, Vol. 7, No. 1 (1971), pp. 63-76.
- 5) Y. Yamada, N. Yoshimura and T. Sakurai; Plastic Stress-strain Matrix and its Application for the Solution of Elastic-plastic Problems by the Finite Element Method, Int. J. Mech. Sci, 10 (1968), pp. 343-354.
- 6) A. Ohtsuka, T. Miyata, S. Nishimura and N. Kasai; The Stretched Zone and COD-criterion on the Fracture, J. Soc. Naval Arch. of Japan, Vol. 136 (1974), pp. 249-257.
- 7) D. S. Dugdale; Yielding of Steel Sheets Containing Slits; J. Mech. Phys. Solids, 8 (1960) pp. 100-104.
- 8) B. A. Bilby, A. H. Cottrell and K. H. Swinden; The Spread of Plastic Yield from a Notch, Proc. Roy. Soc., A279 (1964), pp. 304-314.
- 9) K. Sakai and K. Sakano; A Study on Brittle Fracture Initiation under Combined Modes, J. Soc. Naval Arch. of Japan, Vol. 139 (1976), pp. 257-264.